Mass spectral molecular mapping shows benefits of thermal evaporation in prelithiated silicon-based composite electrodes

Gabriel D. Parker [1], Amanda L. Musgrove [2], Gabriel M. Veith [2], Ivan Matyushov [1], and Xiao-Ying Yu [1,†]

[1] Materials Science and Technology Division, Oak Ridge National Laboratory; matyushovid@ornl.gov, parkergd@ornl.gov
[2] Chemical Sciences Division, Oak Ridge National Laboratory; musgroveal@ornl.gov, veithgm@ornl.gov
[†] Correspondence: yuxiaoying@ornl.gov

Contents

Supporting Figures

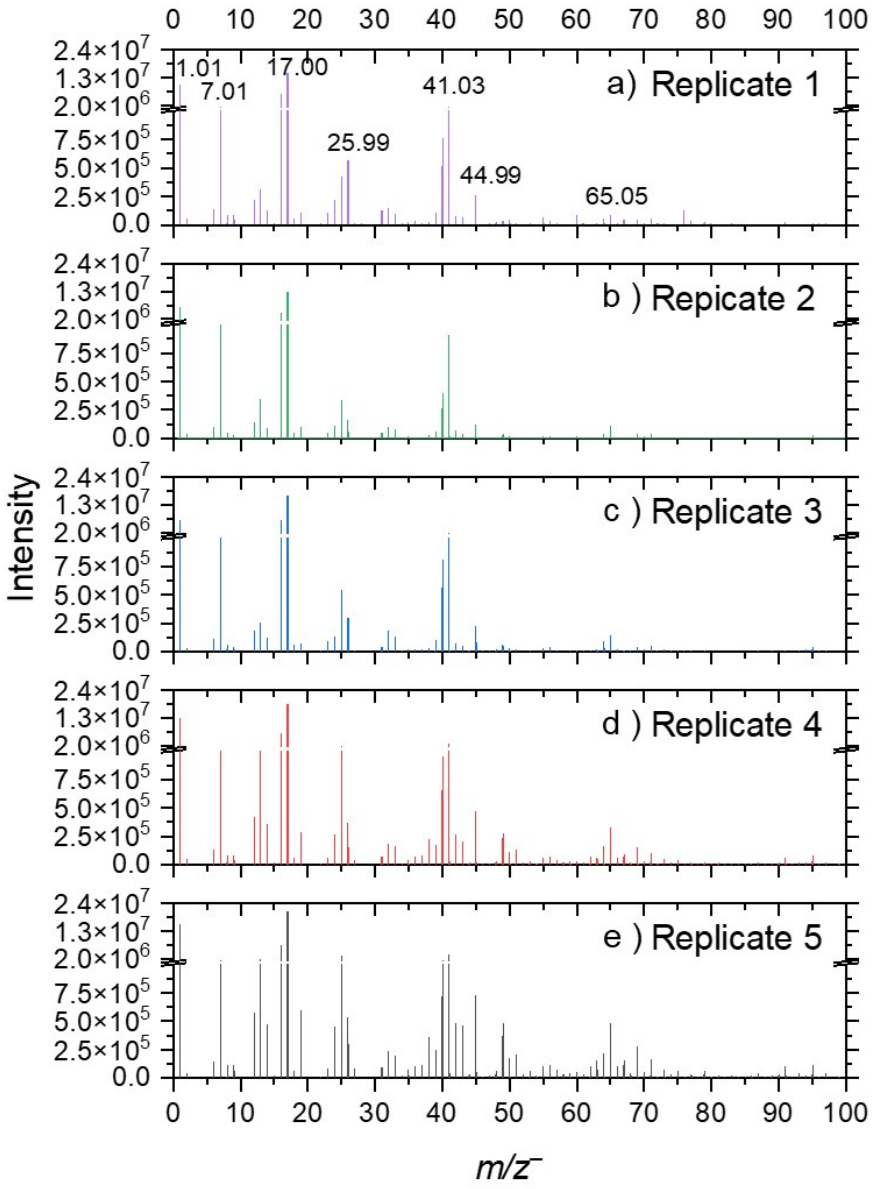

Figure S1. Calibrated SIMS spectra showing reproducibility of SIMS analysis of the inert Ar gas sample in the m/z^- of 0-100 in the negative ion mode.

Figure S1 depicts an example of static ToF-SIMS spectral measurement reproducibility in the m/z^- range of 0 – 100 of the spectra in the negative ion mode. Each replicate is numbered 1-5 with each number corresponding to the first, second, third, fourth, and fifth measurements of this particular sample acquired in the negative ion mode consecutively. Other samples studied in this work have similar spectral reproducibility.

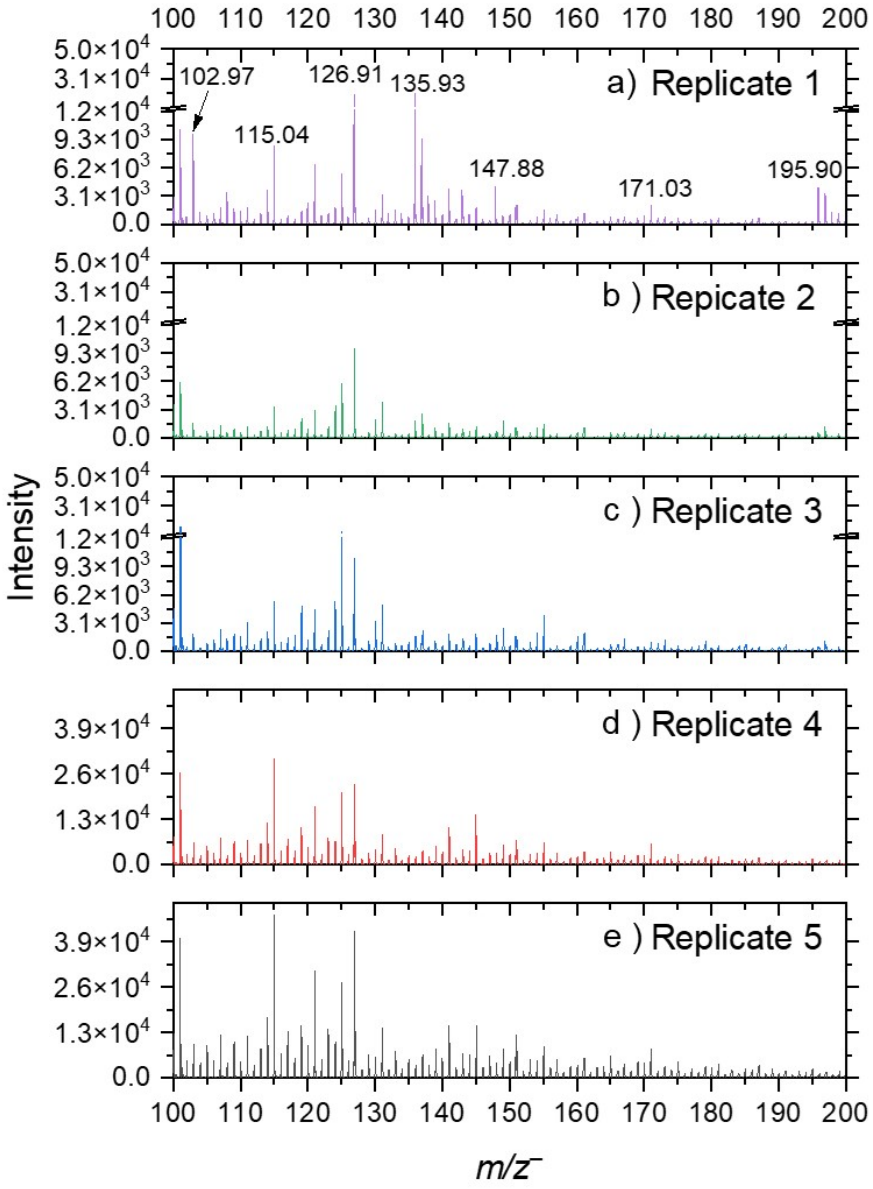

Figure S2. Calibrated SIMS spectra showing reproducibility of SIMS analysis of the inert Ar gas sample in the m/z^- of 100-200 in the negative ion mode.

Figure S2 depicts an example of static ToF-SIMS spectral measurement reproducibility in the m/z^- range of 100 – 200 of the spectra in the negative ion mode. Each replicate is numbered 1-5 with each number corresponding to the first, second, third, fourth, and fifth measurements of this particular sample acquired in the negative ion mode consecutively. Other samples studied in this work have similar spectral reproducibility.

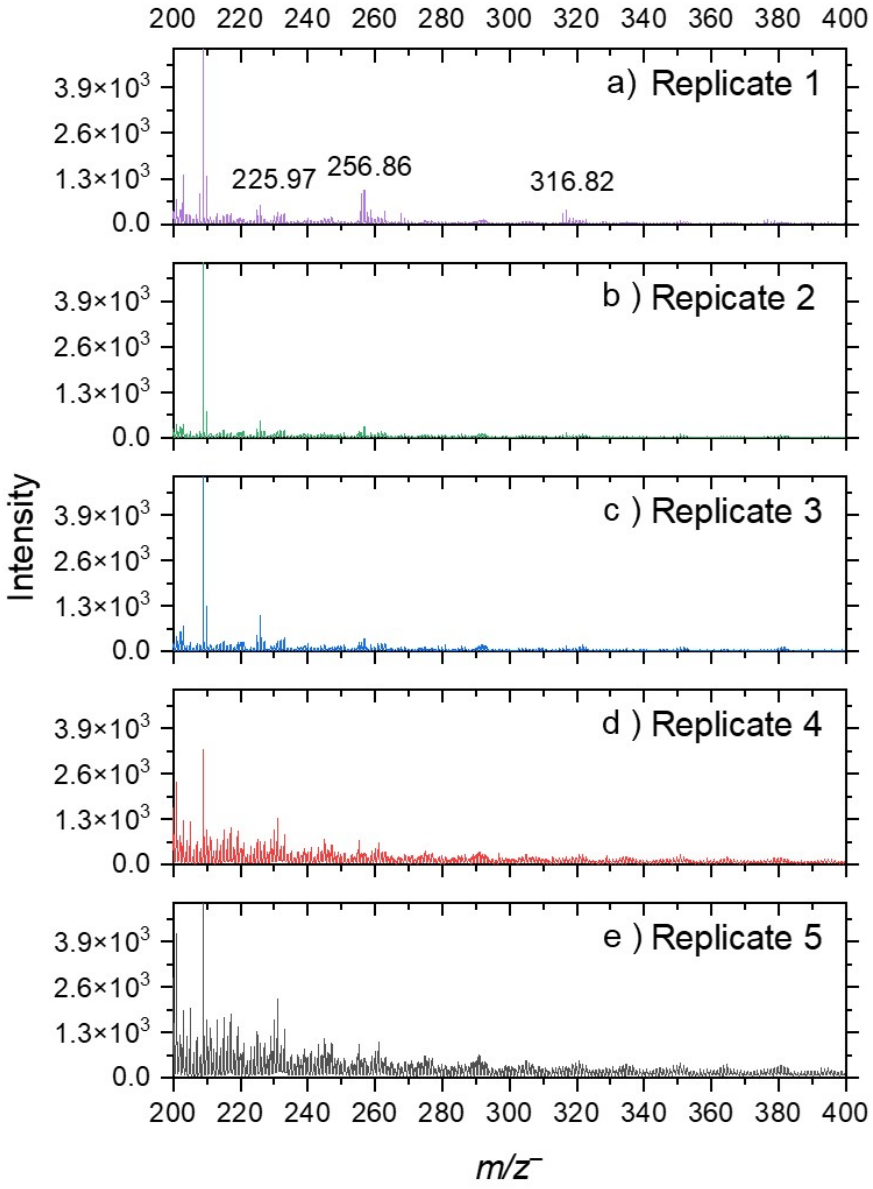

Figure S3. Calibrated SIMS spectra showing reproducibility of SIMS analysis of the inert Ar gas sample in the m/z^- of 200-400 in the negative ion mode.

Figure S3 depicts an example of static ToF-SIMS spectral measurement reproducibility in the m/z^- range of 200 – 400 of the spectra in the negative ion mode. Each replicate is numbered 1-5 with each number corresponding to the first, second, third, fourth, and fifth measurements of this particular sample acquired in the negative ion mode consecutively. Other samples studied in this work have similar spectral reproducibility.

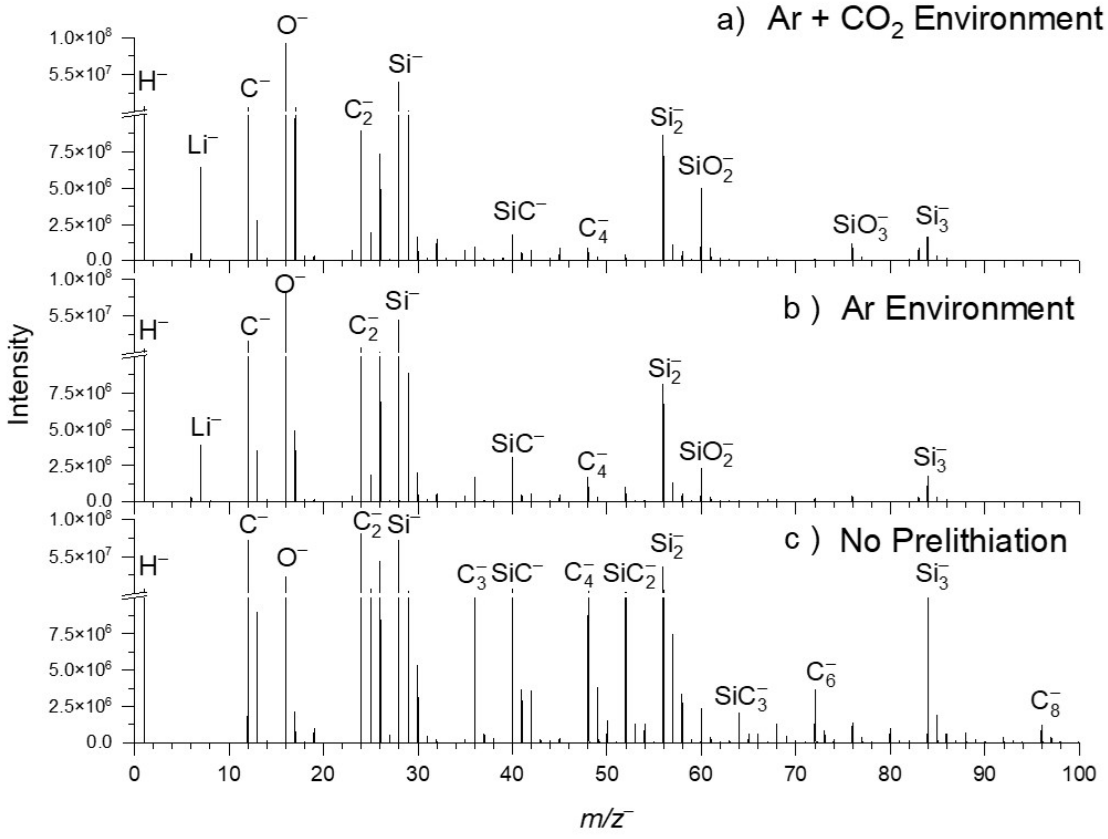

Figure S4. ToF-SIMS mass spectra collected in the negative ion mode within mass range m/z^- 0-100 for prelithiated silicon electrodes housed in Ar + CO_2 environment (a), Ar environment (b), and no prelithiation silicon electrode control sample (c). This mass region shows identifications of $LiSi_2^-$, $LiSiO_2^-$, and $LiSiO_3^-$ peaks found in the prelithiated samples.

Figure S4 shows ToF-SIMS spectra collected for 3 sample times: Ar+CO_2 environment prelithiation conditions (a), Ar environment prelithiation conditions (b), and no prelithiation control samples(c) of the silicon electrodes. This spectral comparison shows many carbon clusters and silicon clusters but due to the high intensity, peaks of interest are not easily recognizable. This mass region shows identifications of $LiSi_2^-$, $LiSiO_2^-$, and $LiSiO_3^-$ peaks found in the prelithiated samples. This figure supports **Figure 2** of the main text, which shows a portion of this mass spectra, m/z^- 50-100. Observed are lithium-silicon/silicate alloy products which indicate lithium penetration within the silicon electrode allowing for metal complexing.

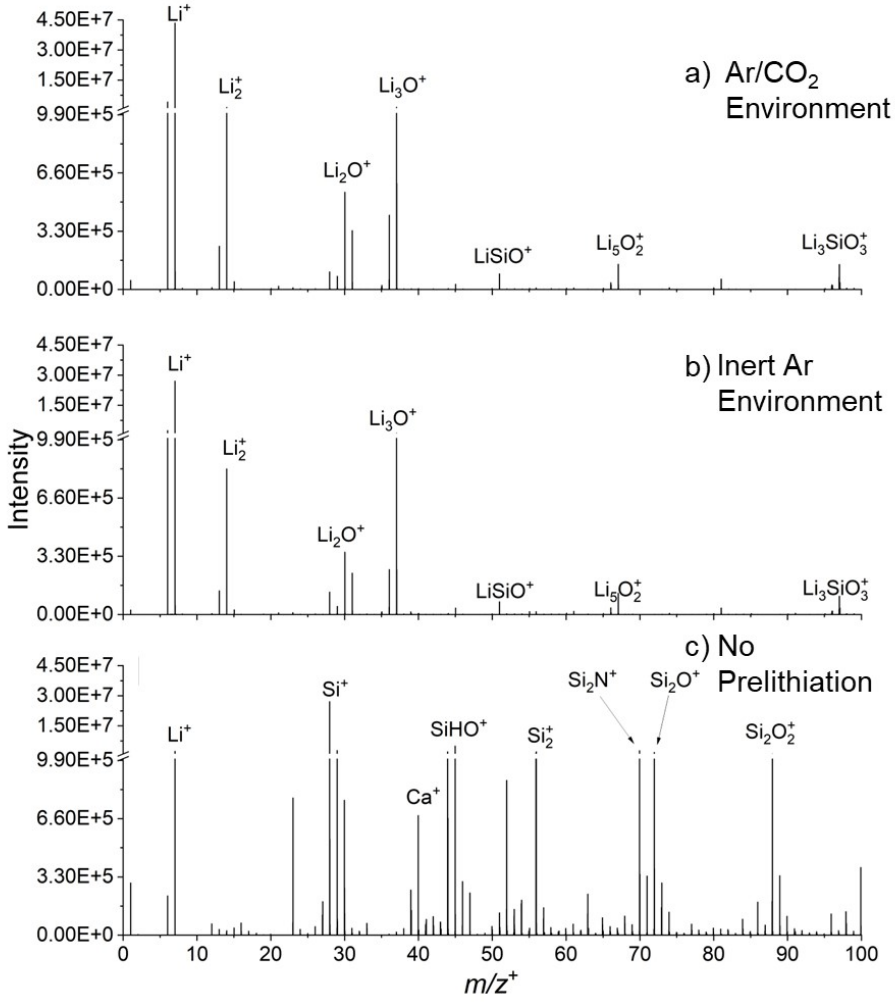

Figure S5. ToF-SIMS mass spectra reconstructed after depth profiling within positive mode showing m/z^+ 0-100 for prelithiated silicon composite electrodes in exposure to Ar/CO_2 environment (a) and an inert Ar environment (b) compared against no prelithiation silicon electrodes(c).

Figure S5 shows dynamic ToF-SIMS spectral comparison results from the positive ion mode of the prelithiation prepared Si electrodes in an Ar/CO_2 environment (a), inert Ar environment (b), and control sample with no prelithiation electrodes (c). The SIMS spectral comparisons are in the mass range of m/z^+ 0 – 100. In the prelithiated samples, primarily lithium-based compounds show both lithium oxides and lithium silicates as prominent peaks. The non-prelithiated samples primarily see silicon-based compounds strongly.

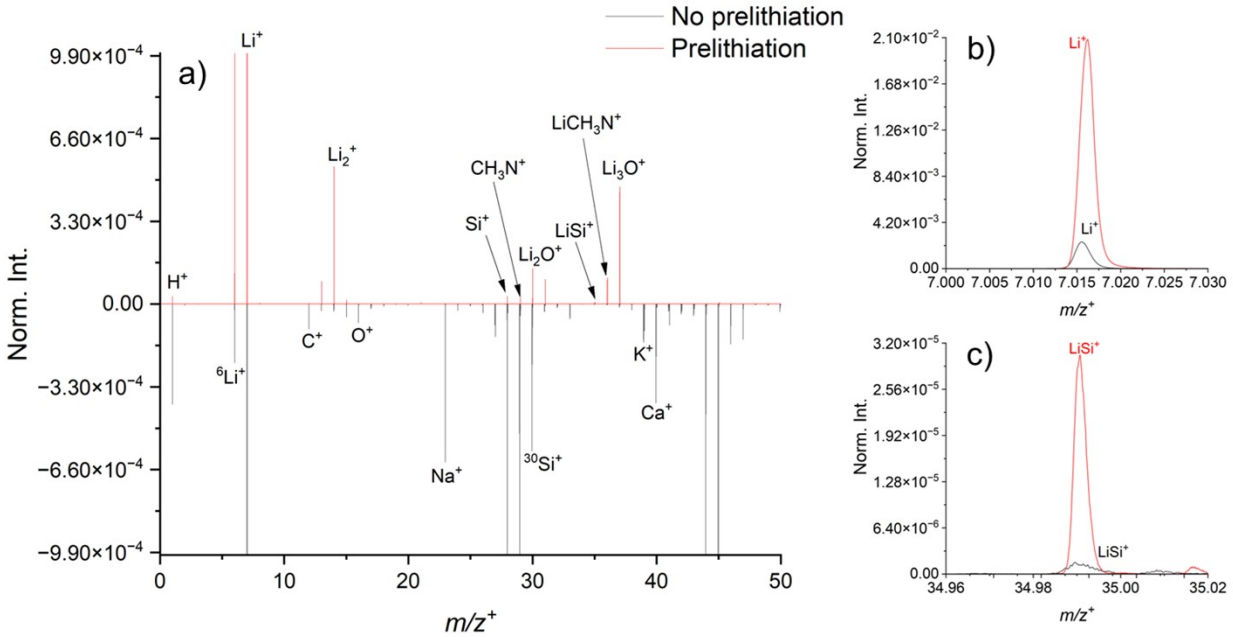

Figure S6. Normalized ToF-SIMS spectra of silicon electrodes with no prelithiation and prelithiation within an Ar/CO_2 environment. (a) Spectra highlighting *m/z*– 0-50 showing lithium, lithium-silicon, and other products of the electrodes. (b) Peak comparison of the lithium observed with no pre-lithiation and after prelithiation. (c) Peak comparison of lithium-silicate with no prelithiation and after prelithiation.

Figure S6 shows normalized ToF-SIMS spectra used for comparing peaks indicative of prelithiated and non-prelithiated silicon electrodes. The results indicate that some lithium is on the surface of the non-prelithiated electrodes, possibly due to manufacturing contamination; however, its count is minimal in comparison with the lithiated sample as shown in **Figure S6b**. Also presented is a small peak identifying lithium-silicon alloy in the non-prelithiated sample depicted in **Figure S6c**. This is most likely an artifact and not a real representation, whereas the prelithiated peak suggests accurate identification of $LiSi^+$ with a mass deviation of 20.4321 ppm.

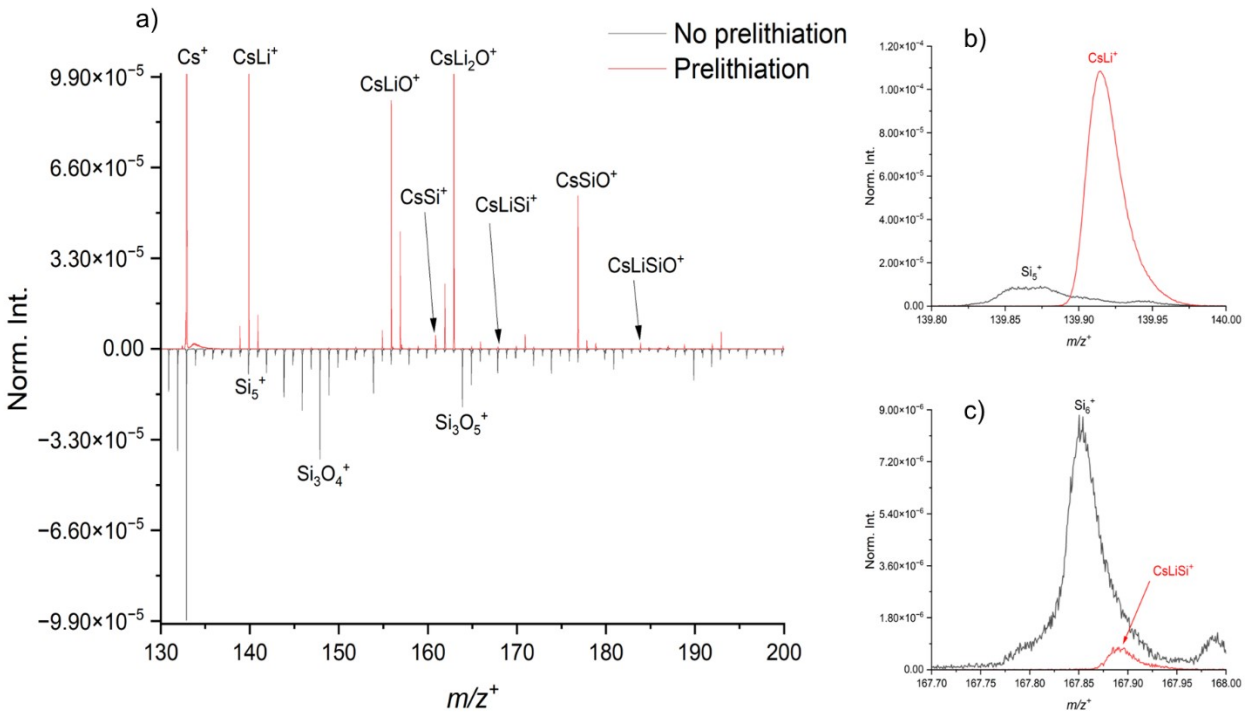

Figure S7. Normalized ToF-SIMS spectra of silicon electrodes with no prelithiation (black) and prelithiation within an Ar/CO_2 environment (red) using the CsM^+ ionization method. (a) Spectra in the m/z^- of 130-200 showing cesium, cesium -lithium, cesium -silicon, and cesium -lithium-silicon products of the electrodes. (b) Peak comparison of the lithium observed with no pre-lithiation and after prelithiation using the CsM^+ method. (c) Peak comparison of lithium-silicate with no prelithiation and after prelithiation using the CsM^+ method.

Figure S7 shows normalized ToF-SIMS spectra reconstructed after depth profiling in the positive ion mode. This spectral comparison shows the principle of the CsM^+ method which utilizes the Cs sputter beam to attach to molecules of interest observed in **Figure S7a**. It is also shown that there is no $CsLi^+$ signal in the control sample, indicating that the products we observe in the prelithiation under Ar/CO_2 environment are a direct result of the thermal evaporation process, as seen in **Figure S7b**. Finally, we observe that lithium-silicon products are not found within the no prelithiation control silicon electrode sample, see **Figure S7c**.

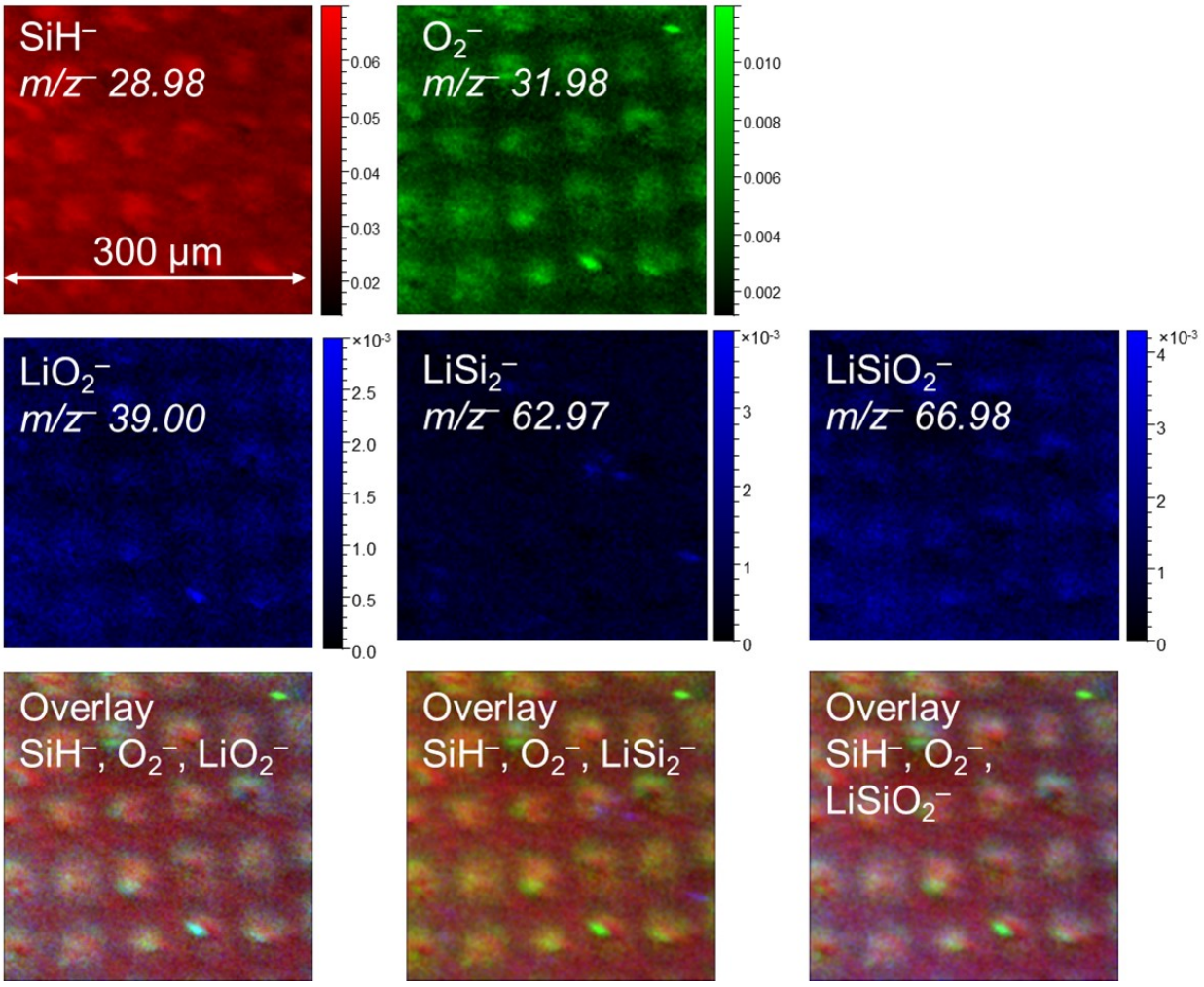

Figure S8. Red, green, blue overlay of SiH^-, O_2^-, and LiO_2^-/$LiSi_2^-$/$LiSiO_2^-$ showing negative areas in the images to be occupied by oxygen in the Ar gas environment prepared electrode sample.

Figure S8 presents the 2D surface images of prelithiated electrodes after preparation in inert Ar gas environment with other peaks present filling the observed voids in the negative mode. These surface chemical maps substantiate the 'mesh-like' pattern of silicon on the surface where lithium signals tend to be more dispersed across the surface. The negative signal areas in the LiO_2^-, $LiSi_2^-$, and $LiSiO_2^-$ images are filled with O_2^-, indicating trapped oxygen. Oxygen indicates less formation of the Li_xSi_y; and it supports the formation of $Li_xSi_yO_z$ alloy in the designated areas provided by the mesh grid.

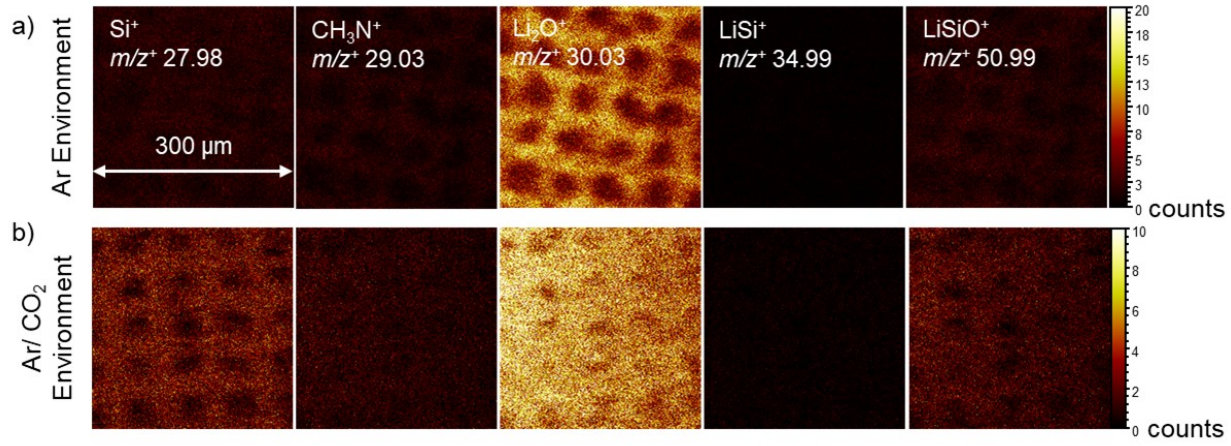

Figure S9. SIMS 2D images in the positive ion mode of electrodes prepared in argon gas environment (a) and Ar/CO_2 gas exposure (b). The analysis area is 300 µm x 300 µm. Their respective intensity scaling is to the right.

Figure S9 presents the surface images of prelithiated electrodes after preparation in inert argon gas (a) and preparation in an Ar/CO_2 gas environment (b) in the positive mode. These surface images substantiate the 'mesh-like' pattern of silicon on the surface, where lithium signals tended to be more dispersed across the surface. These surface 2D images also highlight the presence of Li_xSi_y and $Li_xSi_yO_z$.

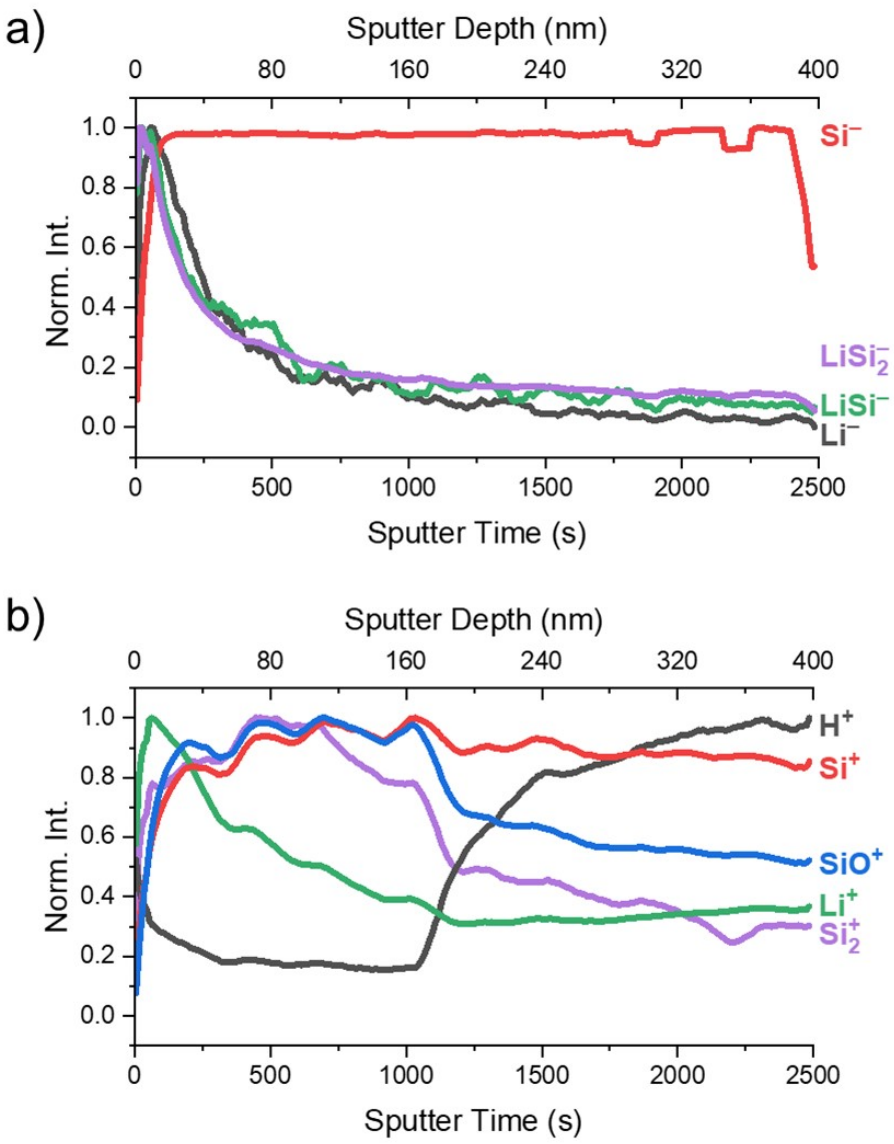

Figure S10. Depth profile plots of sample electrodes with no prelithiation in the negative mode (a) and positive mode (b).

Figure S10 presents the depth profiles of the non-prelithiated electrode samples in the negative (a) and positive mode (b), respectively. Lithium peak can be found in the spectra and depth profiles of both positive and negative polarities; however, lithium and lithium alloys are depleted very quickly. These depth profiles show some lithium contamination was likely in the chamber, which led to some remnant lithium that was detected in large intensities in the positive mode. Even with small amounts of lithium, lithium is highly ionizable and readily observed in the spectra. The depletion of the lithium peak according to the depth profile indicates that the lithium was only at the surface of the electrode. Total sputtering depth was 400 nm. Sputtering done at 0.16 nm/s.

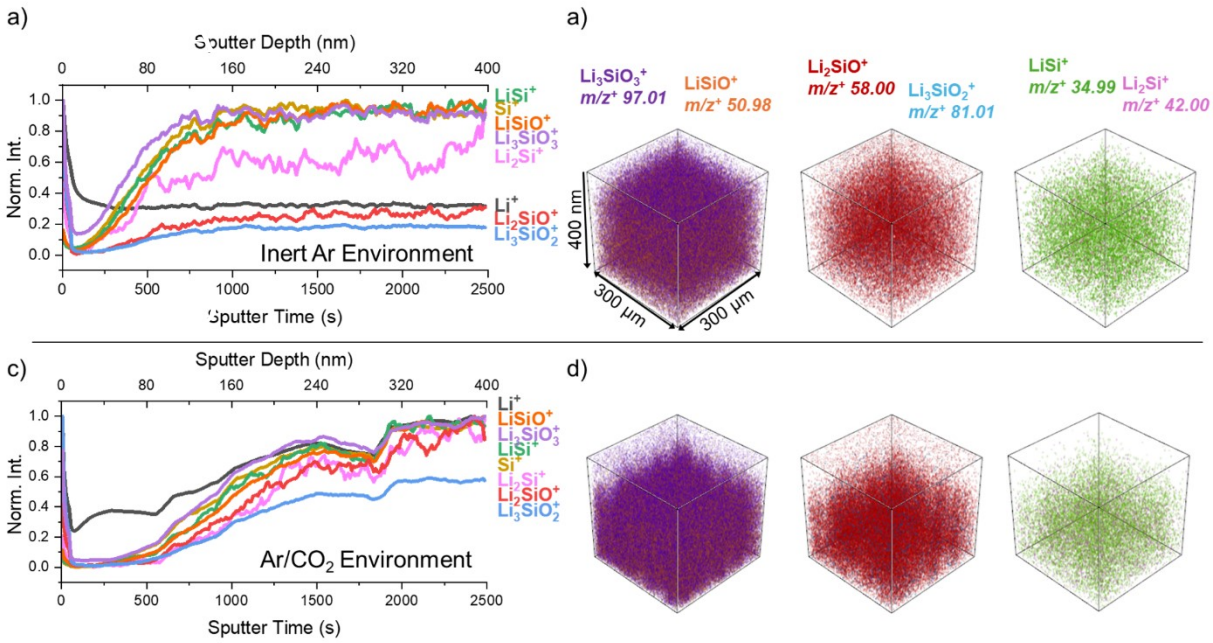

Figure S11. ToF-SIMS depth profiles and overlaying reconstructed 3D SIMS images of the prelithiated electrode materials after exposure to an inert Ar gas environment (a, b) and an Ar/CO_2 gas environment (c, d) in the positive ion mode. Total sputtering depth was 400 nm. Sputtering done at 0.16 nm/s. The same colors are used for identified ions in the depth profiles and 3D images.

Figure S11 presents the depth profiles and overlaying reconstructed 3D SIMS images of the prelithiated electrode samples in the positive mode. Similar to the negative mode in **Figure 4**, both $Li_xSi_yO_z$ and Li_xSi_y compounds are highlighted to show the relative quantities and spatial distributions of lithium alloys and lithium silicates.

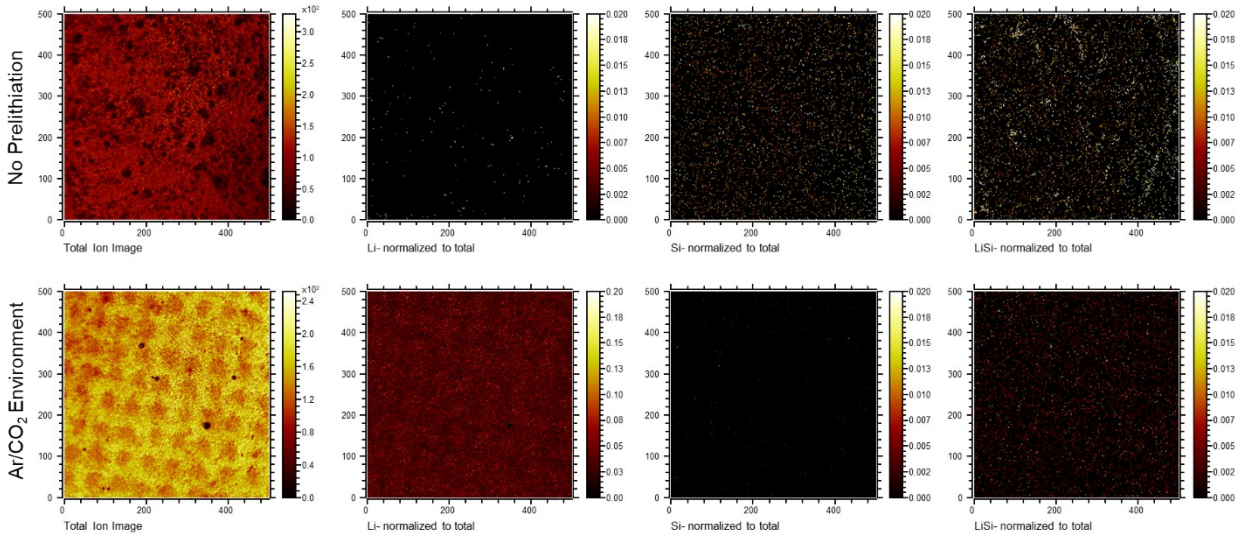

Figure S12. Negative polarity fast images of the anode sample surface for no prelithiation sample and Ar/CO_2 Environment sample showing Li, Si, and LiSi normalized to Total Ion Image within an area of 500 µm × 500 µm.

Figure S12 provides 2D images of the sample surface for no prelithiation and Ar/CO2 passivation anode samples in the negative polarity. High mass resolution spectroscopy mode was used throughout the remainder of the analysis. Imaging mode was not chosen due to low ionization counts within the selected region of interest.

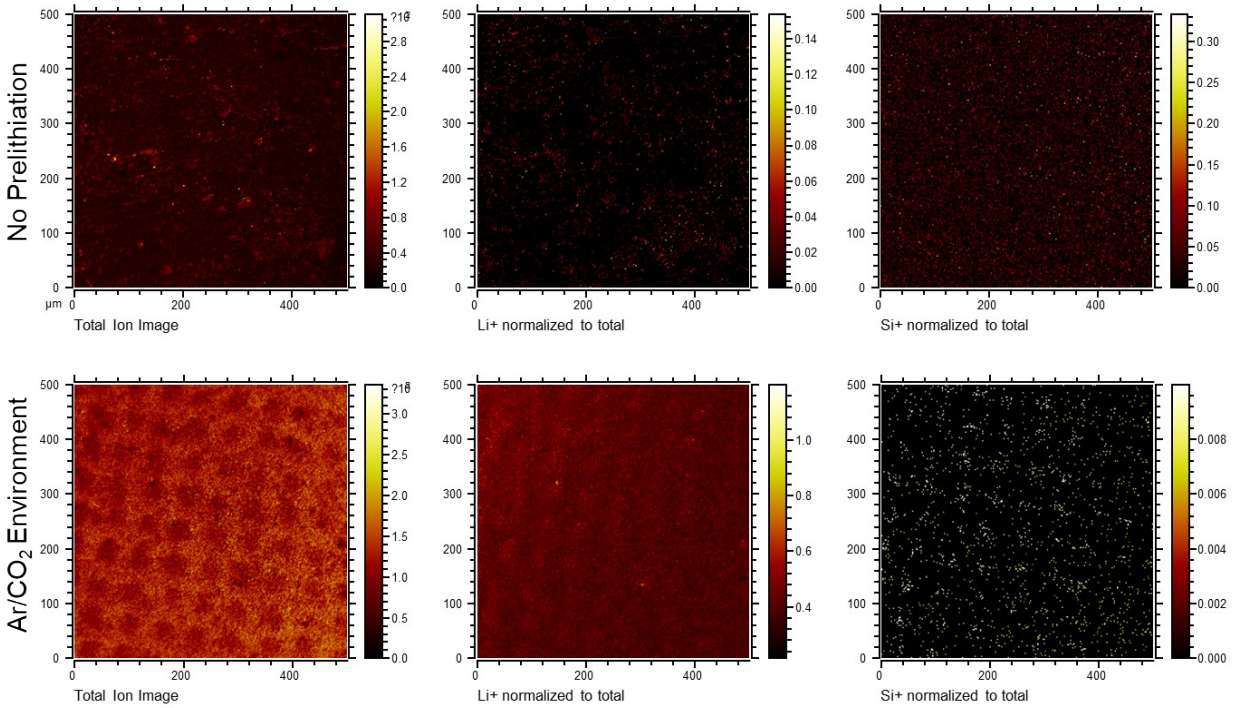

Figure S13. Positive polarity fast images of the anode sample surface for no prelithiation sample and Ar/CO_2 Environment sample showing Li and Si normalized to Total Ion Image within an area of 500 µm × 500 µm.

Figure S13 provides 2D images of the sample surface for no prelithiation and Ar/CO2 passivation anode samples in the positive polarity. High mass resolution spectroscopy mode was used throughout the remainder of the analysis. Imaging mode was not chosen due to low ionization counts within the selected region of interest.

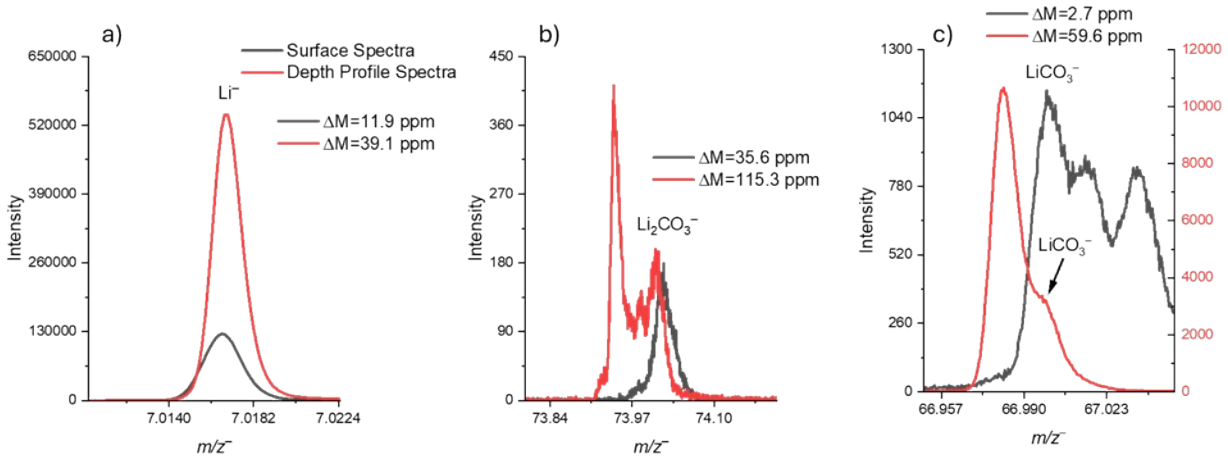

Figure S14. ToF-SIMS spectra showing Ar/CO_2 anode sample surface spectra (black) and depth profile spectra (red) to examine potential lithium carbonate peak identification. (a) Spectra observes Li^-. (b) Spectra observed $Li_2CO_3^-$ with a higher mass deviation for depth profile spectra. (c) Spectra observes prominent lithium carbonate fragment $LiCO_3^-$ is not readily observed in the depth profiling spectra.

Figure S14 shows the surface spectra versus the depth profiling spectra for signs of lithium carbonate within the Ar/CO_2 sample. It is observed that the Li^- peaks for the surface and the depth profile overlap, indicating proper calibration and peak identification. **Figure S14b** shows the lithium carbonate ($Li_2CO_3^-$) molecular spectral comparisons of both surface and depth profile. Here, the surface spectrum in blue has a relatively low mass deviation of 35.6 ppm, indicating that lithium carbonate is at the surface of the anode. However, mass deviation increases to 115.3 ppm from the depth profile reconstructed spectrum. This may indicate that lithium carbonate is no longer identifiable as it is outside our accepted mass deviation of 100 ppm.

Also, the ion counts (cts) for each of these peaks on the surface and from the depth profile are less than 500, which can introduce signal to noise concerns. However, since Li_2CO_3, is the neutral ion, low counts are to be expected. To mitigate these possible interferences, we compare the main fragment, $LiCO_3^-$, which would have a negative charge. In this case, we see a prominent peak with low mass deviation for the surface spectra, indicating lithium carbonate is present at the surface. Its high intensity indicates another peak for the depth profile spectra. However, it is unclear to denote $LiCO_3^-$ in the depth profile spectra. The SIMS spectral results show identification of lithium carbonate at the surface of the Ar/CO_2 anode as expected, offering possible signs of lithium carbonate into the bulk. Further analysis is required to identify lithium carbonate transport into the anode using materials that have gone through cycling.

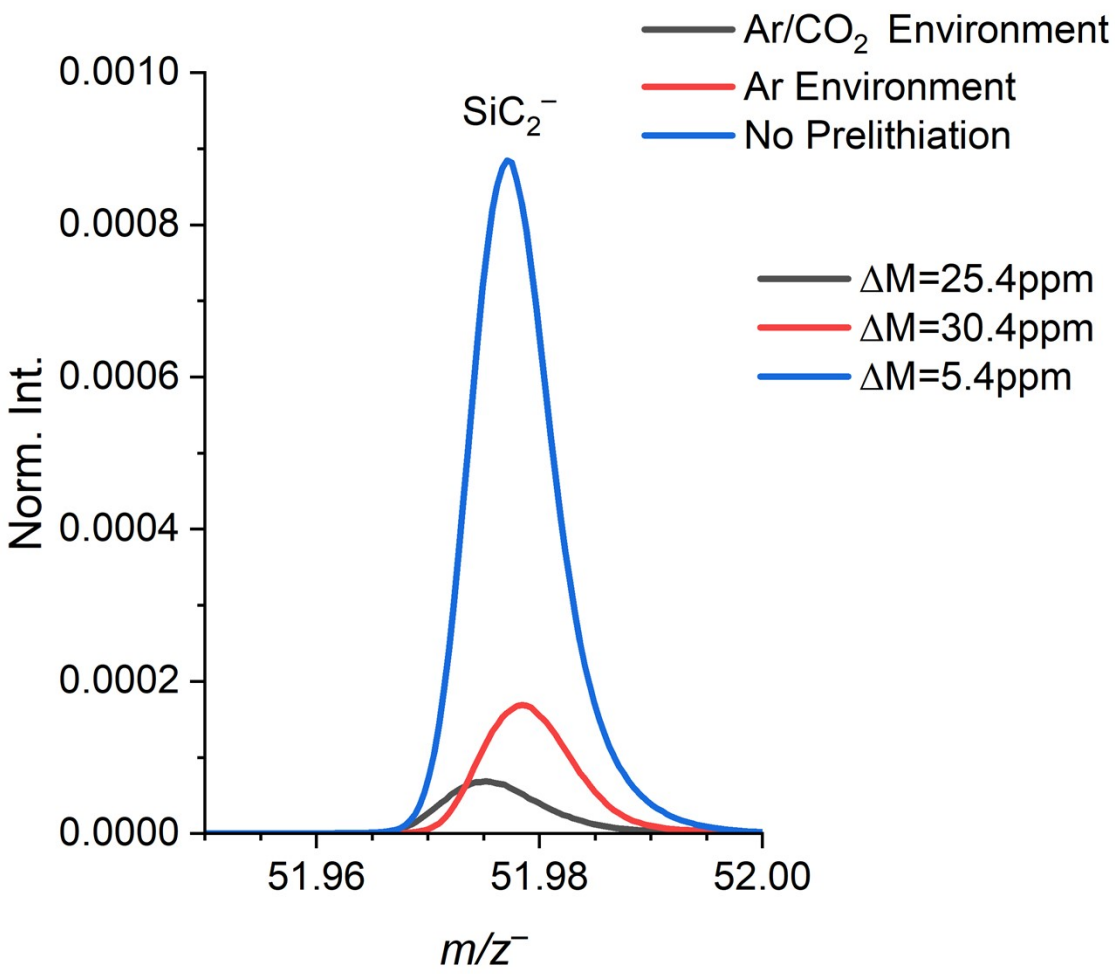

Figure S15. Normalized ToF-SIMS spectra showing comparison of SiC_2^- peak identification for Ar/CO_2 (black), Ar (red), and no prelithiation (blue) samples. Normalization is to total ion counts.

Figure S15 shows ToF-SIMS spectra for SiC_2^- identification for the three samples. Notice that the highest peak intensity for the no prelithiation sample due to the high Si content of the anode. The Ar environment (red) shows the second highest peak intensity, and the Ar/CO_2 sample shows the lowest. It is possible that the silicon content is dependent on how well the prelithiation process proceeds, indicating lower SiC_2 for the sample, which forms LiSi products closer to the sample surface.

Supporting Tables

Table S1: Peak identifications for electrodes in inert Ar gas environment in mass range of m/z^- 0 – 200 in the negative mode.

$m/z^-_{theo.}$	$m/z^-_{obs.}$	ΔM, ppm	Species	Assignment	Ref
1.0084	1.0084	14.4919	H^-	Hydrogen	[1]
7.0164	7.0166	25.4140	Li^-	Lithium	[2]
12.0005	12.0005	6.6797	C^-	Carbon	[2]
15.9960	15.9955	34.4293	O^-	Oxygen	[1]
17.0028	17.0033	27.4558	OH^-	Hydroxide	[1]
18.9985	18.9990	22.6402	F^-	Fluorine	[2]
19.0162	19.0166	16.2238	CLi^-	Lithium Carbide	This work
23.0111	23.0115	16.8126	LiO^-	Lithium Oxide	This work
24.0008	24.0005	12.1750	C_2^-	Carbon cluster	[3]
26.0040	26.0036	13.8899	CN^-	Cyanide	[4]
27.9788	27.9775	45.8948	Si^-	Silicon	[5]
29.9734	29.9743	29.6301	$^{30}Si^-$	Silicon Isotope	[6]
31.0168	31.0166	9.4545	LiC_2^-	Lithium Carbide	This work
31.9719	31.9726	22.1748	S^-	Sulfur	[7]
31.9897	31.9904	22.3089	O_2^-	Oxygen	[4]
33.0207	33.0196	32.0080	$CNLi^-$	Lithium Cyanide	[4]
34.9687	34.9694	18.8991	Cl^-	Chlorine	[7]
34.9928	34.9935	20.4321	$LiSi^-$	Lithium Silicon Alloy	This work
36.0005	36.0005	0.2577	C_3^-	Carbon cluster	[3]
39.0078	39.0064	37.5132	LiO_2^-	Lithium Oxide	[4]
39.9753	39.9775	53.8363	SiC^-	Silicon Carbide	[8]
43.9723	43.9724	1.2760	SiO^-	Silicon Oxide	[7]
46.9954	46.9935	40.3351	$LiSiC^-$	Lithium Silicon Carbide	This work
48.0016	48.0005	21.8377	C_4^-	Carbon Cluster	[3]
50.9897	50.9884	25.9407	$LiSiO^-$	Lithium Silicate	This work
55.9546	55.9544	2.9967	Si_2^-	Silicon Cluster	[9]
59.9685	59.9673	19.3491	SiO_2^-	Silicate	[1]
62.9712	62.9704	12.0339	$LiSi_2^-$	Lithium Silicon Alloy	This work
66.9860	66.9833	40.1563	$LiSiO_2^-$	Lithium Silicate	This work
75.9651	75.9622	38.1093	SiO_3^-	Silicate	[7]
78.9670	78.9653	21.8536	$LiSi_2O^-$	Lithium Silicate	This work
82.9820	82.9782	45.3584	$LiSiO_3^-$	Lithium Silicate	This work
83.9313	83.9313	0.7948	Si_3^-	Silicon Cluster	[10]
90.9477	90.9473	4.1176	$LiSi_3^-$	Lithium Silicon Alloy	This work
97.0131	97.0102	30.0005	$Li_3SiO_3^-$	Lithium Silicate	This work
111.9088	111.9083	4.8205	Si_4^-	Silicon Cluster	[10]
132.9079	132.9060	14.0961	Cs^-	Cesium	[11]
139.8885	139.8852	23.3964	Si_5^-	Silicon Cluster	[10]
160.8810	160.8829	11.9964	$SiCs^-$	Silicon Cesium	[11]
188.8617	188.8598	9.6859	Si_2Cs^-	Silicon Cesium	This work

Note: m/z^- represents the mass-to-charge ratio for negatively charged ions.
[a] $m/z^-_{obs.}$ represents the observed mass to charge ratio.
[b] $m/z^-_{theo.}$ represents the theoretical mass to charge ratio.
[c] ΔM: $\Delta M = 10^6 \times (m/z^-_{obs.} - m/z^-_{theo.})/ m/z^-_{theo.}$ (expressed in ppm).[12]
Peak identification are possibilities identified by SurfaceSpectra software and cross-referenced to literature.

Table S2: Peak identifications for electrodes in Ar/CO_2 gas environment in mass range of m/z^- 0 – 200 in the negative mode.

$m/z^-_{theo.}$	$m/z^-_{obs.}$	ΔM, ppm	Species	Assignment	Ref
1.0084	1.0084	16.2118	H^-	Hydrogen	[1]
7.0166	7.0166	0.1463	Li^-	Lithium	[2]
15.9956	15.9955	9.9358	O^-	Oxygen	[1]
17.0035	17.0033	10.524	OH^-	Hydroxide	[1]
18.9984	18.9990	29.2127	F^-	Fluorine	[2]
19.0163	19.0166	15.8421	CLi^-	Lithium Carbide	This work
23.0112	23.0115	10.2757	LiO^-	Lithium Oxide	This work
24.0008	24.0005	9.0876	C_2^-	Carbon Cluster	[3]
26.0043	26.0036	24.6088	CN^-	Cyanide	[3]
27.9785	27.9775	37.0930	Si^-	Silicon	[5]
29.9737	29.9743	20.5537	$^{30}Si^-$	Silicon Isotope	[6]
31.9902	31.9904	4.6790	O_2^-	Oxygen	[5]
33.0214	33.0196	54.9510	$CNLi^-$	Lithium Cyanide	[5]
34.9694	34.9694	0.0307	Cl^-	Chlorine	[7]
34.9931	34.9935	11.1301	$LiSi^-$	Lithium Silicon Alloy	This work
36.0011	36.0005	15.5977	C_3^-	Carbon Cluster	[3]
39.0054	39.0064	24.4797	LiO_2^-	Lithium Oxide	[4]
39.9752	39.9775	56.2839	SiC^-	Silicon Carbide	[8]
43.9707	43.9724	38.976	SiO^-	Silicon Oxide	[7]
43.9900	43.9904	8.6135	CO_2^-	Carbon Dioxide	[4]
50.9907	50.9884	46.1284	$LiSiO^-$	Lithium Silicate	This work
55.9547	55.9544	5.0058	Si_2^-	Silicon Cluster	[9]
59.9694	59.9673	34.2293	SiO_2^-	Silicate	[1]
62.9720	62.9704	25.4692	$LiSi_2^-$	Lithium Silicon Alloy	This work
66.9891	66.9833	86.9175	$LiSiO_2^-$	Lithium Silicate	This work
78.9689	78.9653	45.9164	$LiSi_2O^-$	Lithium Silicate	This work
82.9836	82.9782	64.3833	$LiSiO_3^-$	Lithium Silicate	This work
83.9317	83.9313	4.3595	Si_3^-	Silicon Cluster	[10]
90.9488	90.9473	16.2503	$LiSi_3^-$	Lithium Silicon Alloy	This work
97.0165	97.0102	64.6421	$Li_3SiO_3^-$	Lithium Silicate	This work
111.9098	111.9083	14.1239	Si_4^-	Silicon Cluster	[10]
120.0143	120.0212	56.9265	$Li_4SiO_4^-$	Lithium Silicate	This work
132.9072	132.9060	8.9012	Cs^-	Cesium	[11]
160.8819	160.8829	6.6668	$SiCs^-$	Silicon Cesium	[11]
174.9095	174.9149	31.255	$CsLi_2Si^-$	Cesium Li_xSi_y Alloy	This work

Note: m/z^- represents the mass-to-charge ratio for negatively charged ions.
[a] $m/z^-_{obs.}$ represents the observed mass to charge ratio.
[b] $m/z^-_{theo.}$ represents the theoretical mass to charge ratio.
[c] ΔM: $\Delta M = 10^6 \times (m/z^-_{obs.} - m/z^-_{theo.})/ m/z^-_{theo.}$ (expressed in ppm).[12]
Peak identification are possibilities identified by SurfaceSpectra software and cross-referenced to literature.

Table S3: Peak identifications for electrodes with no prelithiation done in mass range of m/z^- 0 – 200 in the negative mode.

$m/z^-_{theo.}$	$m/z^-_{obs.}$	ΔM, ppm	Species	Assignment	Ref
1.0083	1.0084	100.9281	H^-	Hydrogen	[1]
7.0161	7.0166	70.7735	Li^-	Lithium	[2]
13.0082	13.0084	17.2199	CH^-	Hydrocarbon	[2]
15.9956	15.9955	9.2559	O^-	Oxygen	[1]
17.0030	17.0033	17.8075	OH^-	Hydroxide	[1]
18.9985	18.9990	24.9460	F^-	Fluorine	[2]
24.0024	24.0005	75.1959	C_2^-	Carbon Cluster	[3]
26.0055	26.0036	71.3543	CN^-	Cyanide	[3]
27.9790	27.9775	54.5032	Si^-	Silicon	[5]
28.9840	28.9853	46.3908	SiH^-	Silicon Hydride	[5]
29.9738	29.9743	18.8002	$^{30}Si^-$	Silicon Isotope	[6]
31.9719	31.9726	23.7079	S^-	Sulfur	[7]
31.9896	31.9904	23.2316	O_2^-	Oxygen	[4]
34.9691	34.9694	7.2828	Cl^-	Chlorine	[7]
36.0014	36.0005	23.2918	C_3^-	Carbon Cluster	[3]
39.9765	39.9775	25.4998	SiC^-	Silicon Carbide	[8]
55.9573	55.9544	51.3752	Si_2^-	Silicon Cluster	[9]
59.9677	59.9673	6.6495	SiO_2^-	Silicate	[1]
67.9560	67.9544	23.8694	Si_2C^-	Silicon Carbide	This work
83.9333	83.9313	23.2241	Si_3^-	Silicon Cluster	[10]
111.9110	111.9083	24.1890	Si_4^-	Silicon Cluster	[10]
132.9092	132.9060	23.8794	Cs^-	Cesium	[11]
139.8896	139.8852	31.7450	Si_5^-	Silicon Cluster	[10]
156.9097	156.9060	23.2884	CsC_2^-	Cesium Carbide	This work
158.9142	158.9091	32.2227	$CsCN^-$	Cesium Cyanide	This work
160.8832	160.8829	1.8890	$SiCs^-$	Silicon Cesium	[10]
167.8700	167.8621	47.2800	Si_6^-	Silicon Cluster	[10]

Note: m/z^- represents the mass-to-charge ratio for negatively charged ions.
[a] $m/z^-_{obs.}$ represents the observed mass to charge ratio.
[b] $m/z^-_{theo.}$ represents the theoretical mass to charge ratio.
[c] ΔM: $\Delta M = 10^6 \times (m/z^-_{obs.} - m/z^-_{theo.}) / m/z^-_{theo.}$ (expressed in ppm).[12]
Peak identification are possibilities identified by SurfaceSpectra software and cross-referenced to literature.

Table S4: Peak identifications for electrodes exposed to inert Ar gas environment in mass range of m/z^+ 0 – 200 in the positive mode.

$m/z^+_{theo.}$	$m/z^-_{obs.}$	ΔM, ppm	Species	Assignment	Ref
6.0153	6.0146	122.3005	$^6Li^+$	Lithium Isotope	[13]
7.0164	7.0155	135.8829	Li^+	Lithium	[2]
12.0002	11.9995	65.8887	C^+	Carbon	[2]
14.0320	14.0315	41.1303	Li_2^+	Lithium Cluster	[2]
19.0162	19.0155	41.4251	CLi^+	Lithium Carbide	This work
27.9774	27.9764	37.7093	Si^+	Silicon	[5]
30.0272	30.0264	26.4020	Li_2O^+	Lithium Oxide	[2]
34.9931	34.9924	20.2620	$LiSi^+$	Lithium Silicon Alloy	This work
37.0447	37.0424	61.9418	Li_3O^+	Lithium Oxide	[2]
42.0113	42.0084	68.4337	Li_2Si^+	Lithium Silicon Alloy	This work
43.9708	43.9713	11.3907	SiO^+	Silicon Oxide	[6]
50.9886	50.9873	25.9150	$LiSiO^+$	Lithium Silicate	This work
55.9541	55.9533	14.4007	Si_2^+	Silicon Cluster	[7]
58.0039	58.0033	10.8447	Li_2SiO^+	Lithium Silicate	This work
67.0689	67.0693	5.5780	$Li_5O_2^+$	Lithium Oxide	This work
81.0177	81.0142	42.9459	$Li_3SiO_2^+$	Lithium Silicate	This work
97.0107	97.0091	16.1818	$Li_3SiO_3^+$	Lithium Silicate	This work
132.9180	132.9049	98.6203	Cs^+	Cesium	[11]
139.9194	139.9209	10.9323	$CsLi^+$	Cesium Lithium	This work
160.8826	160.8818	4.6036	$SiCs^+$	Cesium Silicon	[11]
162.9299	162.9318	11.9185	$CsLi_2O^+$	Cesium Lithium Oxide	This work
176.8771	176.8767	2.0917	$SiOCs^+$	Cesium Silicon Oxide	This work

Note: m/z^+ represents the mass-to-charge ratio for negatively charged ions.
[a] $m/z^+_{obs.}$ represents the observed mass to charge ratio.
[b] $m/z^+_{theo.}$ represents the theoretical mass to charge ratio.
[c] ΔM: $\Delta M = 10^6 \times (m/z^+_{obs.} - m/z^+_{theo.})/ m/z^+_{theo.}$ (expressed in ppm).[12]
Peak identification are possibilities identified by SurfaceSpectra software and cross-referenced to literature.

Table S5: Peak identifications for electrodes exposed to Ar/CO_2 gas environment in mass range of m/z^+ 0 – 200 in the positive mode.

$m/z^+_{theo.}$	$m/z^+_{obs.}$	ΔM, ppm	Species	Assignment	Ref
1.0073	1.0073	428.3205	H^+	Hydrogen	[7]
6.0149	6.0146	186.7328	$^6Li^+$	Lithium Isotope	[13]
7.0160	7.0155	195.4347	Li^+	Lithium	[2]
11.9997	11.9995	85.0338	C^+	Carbon	[2]
14.0316	14.0315	61.6241	Li_2^+	Lithium Cluster	[2]
23.0103	23.0104	17.9083	LiO^+	Lithium Oxide	This work
27.9767	27.9764	22.4159	Si^+	Silicon	[5]
30.0269	30.0264	27.2281	Li_2O^+	Lithium Oxide	[2]
34.9922	34.9924	2.2904	$LiSi^+$	Lithium Silicon Alloy	This work
37.0461	37.0424	99.2428	Li_3O^+	Lithium Oxide	[2]
42.0103	42.0084	40.2687	Li_2Si^+	Lithium Silicon Alloy	This work
49.0258	49.0244	17.6853	Li_3Si^+	Lithium Silicon Alloy	This work
50.9882	50.9873	4.4845	$LiSiO^+$	Lithium Silicate	This work
55.9527	55.9533	27.3037	Si_2^+	Silicon cluster	[9]
58.0050	58.0033	10.4530	Li_2SiO^+	Lithium Silicate	This work
67.0738	67.0693	43.8250	$Li_5O_2^+$	Lithium Oxide	This work
81.0180	81.0155	16.2837	$Li_3SiO_2^+$	Lithium Silicate	This work
89.9958	89.9931	1.7362	$Li_2SiO_3^+$	Lithium Silicate	This work
97.0119	97.0104	5.7104	$Li_3SiO_3^+$	Lithium Silicate	This work
120.0221	120.0201	21.8224	$Li_4SiO_4^+$	Lithium Silicate	This work
132.9208	132.9049	76.6152	Cs^+	Cesium	[11]
139.9213	139.9209	41.2667	$CsLi^+$	Cesium Lithium	This work
155.9168	155.9158	40.1924	$CsLiO^+$	Cesium Lithium Oxide	This work
160.8900	160.8818	3.6907	$SiCs^+$	Silicon Cesium	[11]
176.8810	176.8767	25.5815	$SiOCs^+$	Cesium Silicon Oxide	This work

Note: m/z^+ represents the mass-to-charge ratio for negatively charged ions.
[a] $m/z^+_{obs.}$ represents the observed mass to charge ratio.
[b] $m/z^+_{theo.}$ represents the theoretical mass to charge ratio.
[c] ΔM: $\Delta M = 10^6 \times (m/z^+_{obs.} - m/z^+_{theo.}) / m/z^+_{theo.}$ (expressed in ppm).[20]
Peak identification are possibilities identified by SurfaceSpectra software and cross-referenced to literature.

Table S6: Peak identifications for electrodes with no prelithiation done in mass range of m/z^+ 0 – 200 in the positive mode.

$m/z^+_{theo.}$	$m/z^-_{obs.}$	ΔM, ppm	Species	Assignment	Ref
1.0076	1.0073	297.3367	H^+	Hydrogen	[3]
7.0162	7.0155	100.6255	Li^+	Lithium	[2]
8.0239	8.0233	77.3767	LiH^+	Lithium Hydride	[4]
12.0003	11.9995	74.1822	C^+	Carbon	[2]
15.0241	15.0229	76.2118	CH_3^+	Hydrocarbon	[2]
15.9952	15.9944	53.2683	O^+	Oxygen	[1]
17.0028	17.0022	33.6237	OH^+	Hydroxide	[1]
22.9902	22.9892	42.4414	Na^+	Sodium	[7]
24.0000	23.9995	24.8880	C_2^+	Carbon Cluster	[3]
27.9784	27.9764	73.6707	Si^+	Silicon	[5]
28.9843	28.9842	1.9659	SiH^+	Silicon Hydride	[5]
29.9741	29.9732	29.0097	$^{30}Si^+$	Silicon Isotope	[6]
31.9899	31.9893	20.6040	O_2^+	Oxygen	[4]
34.9925	34.9924	2.5149	$LiSi^+$	Lithium Silicon Alloy	This work
35.9998	35.9995	10.6078	C_3^+	Carbon Cluster	[3]
38.9627	38.9632	12.7609	K^+	Potassium	[14]
39.9605	39.9620	37.9885	Ca^+	Calcium	[14]
41.0412	41.0386	62.9338	$C_3H_5^+$	Hydrocarbon	[5]
43.9705	43.9713	17.1068	SiO^+	Silicon Oxide	[7]
53.9809	53.9795	26.3407	$SiCN^+$	Silicon Carbon Nitride	This work
59.9656	59.9662	9.6435	SiO_2^+	Silicate	[1]
83.9297	83.9302	6.2940	Si_3^+	Silicon Cluster	[10]
111.9013	111.9072	52.7227	Si_4^+	Silicon Cluster	[10]
132.9036	132.9049	9.9765	Cs^+	Cesium	[11]

Note: m/z^+ represents the mass-to-charge ratio for negatively charged ions.
[a] $m/z^+_{obs.}$ represents the observed mass to charge ratio.
[b] $m/z^+_{theo.}$ represents the theoretical mass to charge ratio.
[c] ΔM: $\Delta M = 10^6 \times (m/z^+_{obs.} - m/z^+_{theo.}) / m/z^+_{theo.}$ (expressed in ppm).[12]
Peak identification are possibilities identified by SurfaceSpectra software and cross-referenced to literature.

References

1. L. Yang, Y.-Y. Lua, G. Jiang, B. J. Tyler and M. R. Linford, *Analytical Chemistry*, 2005, **77**, 4654-4661.
2. N. Gauthier, C. Courrèges, J. Demeaux, C. Tessier and H. Martinez, *Appl. Surf. Sci.*, 2020, **501**, 144266.
3. N. Mayama, Y. Miura, K. Misawa, A. Takami, T. Sakamoto and M. Fujii, *Anal. Sci.*, 2013, **29**, 479-482.
4. Y. Zhao, S.-K. Otto, T. Lombardo, A. Henss, A. Koeppe, M. Selzer, J. Janek and B. Nestler, *ACS Appl. Mater. Interfaces.*, 2023, **15**, 50469-50478.
5. V. A. Brown, D. A. Barrett, P. N. Shaw, M. C. Davies, H. J. Ritchie, P. Ross, A. J. Paul and J. F. Watts, *Surf. Interface Anal.*, 1994, **21**, 263-273.
6. M. N. Drozdov, Y. N. Drozdov, D. A. Pryakhin, V. I. Shashkin, P. G. Sennikov and H.-J. Pohl, *Bull. Russ. Acad. Sci.: Phys.*, 2010, **74**, 75-77.
7. A. Rossi, B. Elsener, G. Hähner, M. Textor and N. D. Spencer, *Surf. Interface Anal.*, 2000, **29**, 460-467.
8. S. Richter, K. Kaufmann and C. Hagendorf, *Phys. Status Solidi C*, 2011, **8**, 796-799.
9. A. Benninghoven, *Angew. Chem. Int. Ed.*, 1994, **33**, 1023-1043.
10. M. Perego, S. Ferrari, M. Fanciulli, G. Ben Assayag, C. Bonafos, M. Carrada and A. Claverie, *SIMS XIV*, 2004, **231-232**, 813-816.
11. J. Brison, R. G. Vitchev and L. Houssiau, *Nucl. Instrum. Methods Phys. Res., B*, 2008, **266**, 5159-5165.
12. X.-Y. Yu, C. Yang, J. Gao, J. Xiong, X. Sui, L. Zhong, Y. Zhang and J. Son, *Front. Chem.*, 2023, **11**, 1253685.
13. X.-Y. Yu, J. Yao, B. Matthews, S. R. Spurgeon, S. Riechers, G. Sevigny, Z. Zhu, W. Jiang and W. Luscher, *J. Mater. Res. Technol.*, 2021, **14**, 475-483.
14. M. A. Douglas and P. J. Chen, *Surf. Interface Anal.*, 1998, **26**, 984-994.